

# Self-trapping and switching of solitonic pulses in mismatched dual-core highly nonlinear fibers

Nguyen Viet Hung<sup>a</sup>, Le Xuan The Tai<sup>b</sup>, Mattia Longobucco<sup>c,d</sup>, Ryszard Buczyński<sup>c,d</sup>, Ignac Bugár<sup>e,f</sup>, Ignas Astrauskas<sup>e</sup>, Audrius Pugžlys<sup>e</sup>, Andrius Baltuška<sup>e</sup>, Boris Malomed<sup>g,h</sup>, Marek Trippenbach<sup>i</sup>

<sup>a</sup>*International Training Institute for Materials Science (ITIMS), Hanoi University of Science and Technology (HUST), No 1 - Dai Co Viet Str., Hanoi, Vietnam*

<sup>b</sup>*Faculty of Physics, Warsaw University of Technology, Koszykowa 75, Warsaw, 00-662, Poland*

<sup>c</sup>*Department of Glass, Łukasiewicz Research Network - Institute of Microelectronics & Photonics, Aleja Lotników 32/46, Warsaw, 02-668, Poland*

<sup>d</sup>*Department of Photonics, Faculty of Physics, University of Warsaw, Pasteura 5, Warsaw, 02-093, Poland*

<sup>e</sup>*Photonics Institute, TU Wien, Gußhausstraße 25-29, Vienna, 1040, Austria*

<sup>f</sup>*Department of Chemistry, University of Ss. Cyril and Methodius in Trnava, Nám. J. Herdu 2, Trnava, 917 01, Slovakia*

<sup>g</sup>*Department of Physical Electronics, School of Electrical Engineering, Faculty of Engineering, Center for Light-Matter Interaction, Tel Aviv University, Tel Aviv 69978, Israel*

<sup>h</sup>*Instituto de Alta Investigación, Universidad de Tarapacá, Casilla 7D, Arica, Chile*

<sup>i</sup>*Institute of Theoretical Physics, Faculty of Physics, University of Warsaw, Pasteura 5, Warsaw, 02-093, Poland*

---

## Abstract

We investigate experimentally and theoretically effects of the inter-core propagation mismatch on nonlinear switching in dual-core high-index-contrast soft-glass optical fibers. Incident femtosecond pulses of various energy are fed into a single ("straight") core, to identify transitions between different dynamical regimes, *viz.*, inter-core oscillations, self-trapping in the cross core, and retaining the pulse in the straight core. The transfer between channels, which has solitonic character, is controlled by the pulse's energy. A model based on the system of coupled nonlinear Schrödinger equations reveals the effect of the mismatch parameter and pulse duration on the diagram of the various

---

*Email address:* hung.nguyenviet@itims.edu.vn (Nguyen Viet Hung)

energy dependent dynamical regimes. Optimal values of the mismatch and pulse width, which ensure stable performance of the nonlinear switching, are identified. The theoretical predictions are in agreement with experimental findings.

*Keywords:* Mismatched dual-core optical fibers, soft glass optical fibers, nonlinear fiber optics, all-optical switching, asymmetric coupler.

---

## 1. Introduction

The concept of nonlinear directional couplers based on dual-core fibers (DCFs) was introduced theoretically in the early 1980s [1, 2]. Since then, considerable efforts were devoted to the characterization and optimization of their performance [3, 4, 5]. New perspectives had emerged with the advent of the photonic-crystal-fiber technology, which offers appropriate conditions for efficient coherent spectral broadening, especially in the case of anomalous group-velocity dispersion (GVD) [6, 7]. Additionally, theoretical work has predicted that the asymmetry between the cores in the fiber may be advantageous for the nonlinear switching dynamics in the soliton propagation regime [8, 9, 10]. The asymmetry needs to be carefully applied, as an excessively high value of the inter-core index mismatch destroys the coupling between parallel cores [11]. Therefore, fabrication of photonic crystal fibers (PCFs) with appropriate properties is a challenging task. Using the PCF production technology, it is hard to create DCF structures with sufficiently low asymmetry. As an alternative, a promising candidate for ultrafast pulse steering was proposed recently, *viz.*, a dual-core high-index-contrast optical fiber made of soft glass [12]. The simple cladding of such a fiber, surrounding a highly nonlinear core, ensures, simultaneously, high nonlinearity, tight field localization, and a low level of dual-core asymmetry at significantly simplified technology [13]. The applicability of this technology was demonstrated both in a vicinity of 1700 nm [12] and in the C-band [13]. Parallel to the experimental work, the understanding of the physical mechanism behind this setting has advanced with the help of extensive numerical studies [14, 15, 16]. The multiple switching performance, observed under the action of the monotonous increase of the pulse's energy, has confirmed the role of the soliton self-trapping in the specialty highly nonlinear fiber [12, 13]. The exchangeable self-trapping in both cores is the key mechanism in the studied dynamical regimes, which could be simulated using a relatively simple model. The application for real

experimental conditions has revealed very good agreement between the experimental and theoretical results [13]. However, the role of asymmetry of the dual-core structure was not investigated experimentally or theoretically. In this work we report new findings, obtained by exciting both cores in the experiment, and introducing an effective refractive-index mismatch between the cores in the numerical studies. The reported results provide an essential step forward in the design of DCFs with an enhanced potential for applications, such as multiplexers [17] and nonlinear all-optical switches [18].

## 2. The theoretical model

The model is based on the system of linearly coupled nonlinear Schrödinger equations (NLSEs) [19, 20, 21], written for complex envelopes  $A(z, t)$  of electromagnetic waves in the mismatched cores of the DCF,

$$\begin{aligned} \partial_z A_1 + \beta_{11} \partial_t A_1 + \frac{i\beta_{21}}{2} \partial_{tt} A_1 = i\kappa_{12}^0 A_2 - \kappa_{12}^1 \partial_t A_2 \\ + i\delta A_1 + i\gamma_1 |A_1|^2 A_1, \end{aligned} \quad (1)$$

$$\begin{aligned} \partial_z A_2 + \beta_{12} \partial_t A_2 + \frac{i\beta_{22}}{2} \partial_{tt} A_2 = i\kappa_{21}^0 A_1 - \kappa_{21}^1 \partial_t A_1 \\ - i\delta A_2 + i\gamma_2 |A_2|^2 A_2. \end{aligned} \quad (2)$$

All coefficients were evaluated at central frequency  $\omega_0$  corresponding to the wavelength  $\lambda_0 = 1700$  nm of the excitation pulses for the specific fiber employed in our experimental study, using a mode solver from Lumerical. The two fiber cores have a nearly hexagonal shape, with the  $3.1 \mu\text{m}$  distance between their centers and the effective mode area of  $1.66 \mu\text{m}^2$  at 1700 nm [13]. The frequency-independent coupling coefficients  $\kappa_{12}^0$  and  $\kappa_{21}^0$  are, respectively:

$$\kappa_{12}^0 = \frac{2\pi^2}{\lambda_0^2 \beta} \int \int_{-\infty}^{\infty} (n^2 - n_1^2) F_1^* F_2 dx dy, \quad (3)$$

$$\kappa_{21}^0 = \frac{2\pi^2}{\lambda_0^2 \beta} \int \int_{-\infty}^{\infty} (n^2 - n_2^2) F_2^* F_1 dx dy. \quad (4)$$

where functions  $F_1(x, y)$  and  $F_2(x, y)$  are field-distribution profiles of fundamental modes in each core, subject to the normalized conditions,

$$\int \int_{-\infty}^{\infty} |F_1(x, y)|^2 dx dy = \int \int_{-\infty}^{\infty} |F_2(x, y)|^2 dx dy = 1,$$

$\kappa_{21}^0$  and  $\kappa_{12}^0$  are the first-order expansion of the frequency dependent coupling coefficient  $\kappa$  (coupling dispersion).  $n_1$  and  $n_2$  are refractive indices of the two cores, and  $n(x, y)$  is the refractive-index profile of the DCF [4]. In our case, the refractive indices of both cores are identical (the PBG08 glass was used as the core material, with  $n_{1,2} = 1.9$ ), while the asymmetry is underlain by a difference in shapes of the cores. Beyond the core, the refractive index is uniform, corresponding to the cladding material, *viz.*, UV710 glass ( $n = 1.52$ ). The asymmetry parameter is

$$\delta = \frac{1}{2}(\beta_{01} - \beta_{02}) \quad (5)$$

where  $\beta_{0m}$  are propagation constants at  $\lambda_0$  in the individual channel ( $m = 1, 2$ ). The nonlinear Kerr coefficients are:

$$\gamma_m = \frac{2\pi\tilde{n}_2}{\lambda_0} \int \int_{-\infty}^{\infty} |F_m(x, y)|^4 dx dy \quad (6)$$

where  $\tilde{n}_2 = 4.3 \times 10^{-19} \text{ m}^2/\text{W}$  is the nonlinear index of refraction of the PBG08 glass used as the core material, which is about 20 times higher than in silica.

### 3. Rescaling the physical parameters, and an exact solution for the linearized system

In the simulations, we used rescaled parameters and noticed that in our fiber differences between the cores in terms of the coupling coefficients are negligible, therefore:  $\kappa_{12}^{0,1} \approx \kappa_{21}^{0,1} = \kappa_{0,1}$ . We define dimensionless parameters for time, distance, and amplitude:  $\tau = t\sqrt{\kappa_0/|\beta_{21}|} = t/t_0$ ,  $\zeta = z(2\kappa_0/\pi) = z/z_0$ , and  $\Psi = \sqrt{\gamma/\kappa_0}A$ , and cast equations (1)-(2) in the following form (notice that we have defined unit of time  $t_0$  and unit of length  $z_0$ , which will later be related to the pulse duration and propagation length):

$$-i\partial_\zeta \Psi_1 = i\epsilon\partial_T \Psi_2 - i(\alpha_2 - \alpha_1)\partial_T \Psi_1 + \frac{1}{2}\partial_{TT} \Psi_1 + \sigma\Psi_1 + |\Psi_1|^2\Psi_1 + \Psi_2, \quad (7)$$

$$-i\partial_\zeta \Psi_2 = i\epsilon\partial_T \Psi_1 + \frac{\alpha}{2}\partial_{TT} \Psi_2 - \sigma\Psi_2 + |\Psi_2|^2\Psi_2 + \Psi_1. \quad (8)$$

where  $\alpha_1 = \beta_{11}/\sqrt{\kappa_0|\beta_{21}|}$ ,  $\alpha_2 = \beta_{12}/\sqrt{\kappa_0|\beta_{21}|}$ ,  $\alpha = |\beta_{22}|/|\beta_{21}|$ ,  $\epsilon = \kappa_1/\sqrt{\kappa_0|\beta_{21}|}$ , and the mismatched parameter:  $\sigma = (\beta_{01} - \beta_{02})/(2\kappa_0)$  and we used the retarded time  $T = \tau - \alpha_2\zeta$ . In the experiments, we have achieved the best

Table 1: Optical parameters of the dual-core fiber, which were utilized for the numerical study of the nonlinear propagation. The parameters, corresponding to the fiber used in the experiment, were produced with the help of the mode-solver at the carrier wavelength of 1700 nm.

Physical quantity	1st core	2nd core	Units
$n_{eff}$	1.77766	1.77719	
$\beta_0$	$6.56172 \times 10^6$	$6.55996 \times 10^6$	$1/m$
$\beta_1$	$6.58061 \times 10^{-9}$	$6.58085 \times 10^{-9}$	$s/m$
$\beta_2$	$-9.886149 \times 10^{-26}$	$-9.886149 \times 10^{-26}$	$s^2/m$
$\gamma$	0.85338	0.85584	$1/(W.m)$
$\kappa_0$	1017.8058	1017.8058	$1/m$
$\kappa_1$	$-1.49662 \times 10^{-13}$	$-1.49662 \times 10^{-13}$	$s/m$

results at  $\lambda_0 = 1700$  nm, hence all the parameters refer to this wavelength. Below we present a table with effective values at this wavelength.

Using the values reported in Table 1,  $\alpha_1 = 656.0245871$ ,  $\alpha_2 = 656.0485128$ ,  $\epsilon = -0.01492$ . Here the last parameter is related to the dispersive character of the coupling coefficient. Even though it seems small in absolute value, it is crucial for pulse propagation dynamics.

Due to the small difference between the GVD and nonlinearity in both cores, average values were used for the numerical modeling, *viz.*,  $\beta_2 = -9.886149 \times 10^{-26} \text{ s}^2\text{m}^{-1}$  and  $\gamma = 0.85461 \text{ W}^{-1}\text{m}^{-1}$  and  $\alpha = 1$ . It is worth mentioning that the negative value of  $\beta_2$  means the anomalous sign of GVD of the fiber at 1700 nm, hence solitonic propagation may be expected, initiated by the ultrafast excitation pulse in such a highly nonlinear fiber.

The high-index core (the first core) is the one with a high group velocity, and the low-index core (the second core) with a low group velocity.

The units of propagation length and time for our experimental conditions can be evaluated to be

$$z_0 = \frac{\pi}{2\kappa} = 1.54 \text{ mm} \quad (9)$$

$$t_0 = \sqrt{|\beta_2|/\kappa} = 9.86 \text{ fs} \quad (10)$$

The length of our fiber was about 18 mm, which corresponds to the dimensionless propagation distance of 18.3. It is worth mentioning that, after the completion of full periods of inter-core oscillations in the linear propaga-

tion regime, the initially excited core stays dominant. In particular, the 18 mm propagation length, representing about 6 periods, maintains this effect, as confirmed experimentally by monitoring the field distribution in area of the both cores at the output.

The asymmetry parameter  $\sigma$  plays an important role in the dynamics of the pulse propagation in the fiber. Considering the difference between the optical parameters of the two cores presented in Table 1 is obvious that the most “influential” coefficient is the propagation constant. The group-velocity mismatch, determined by the frequency derivative of  $\beta_0$ , is more than an order of magnitude lower, and the GVD mismatch between the cores is completely negligible. For this reason, the group-velocity difference was fixed, and only  $\sigma = (\beta_{01} - \beta_{02})/(2\kappa)$  was varied in the course of the simulations, as it represents the dominant effect of the mismatch. Therefore, in our study, the impact of the asymmetry is investigated by systematically increasing the value of  $\sigma$  from 0, which represents the symmetric coupler without any mismatch. The asymmetry parameter is increased up to the level where the nonlinear switching is still possible, but with lower sensitivity to small changes of the input energy, in terms of the output-port-dominance exchange.

We have also examined the effect of the pulse’s shape and concluded that the results are practically the same when sech or Gaussian pulses are used. The pulse-width effect was examined experimentally in the range between 110 and 150 fs, which is sufficiently broad, taking into consideration that the soliton order increases linearly with the increasing width [4]. Careful complex amplitude-phase diagnostics was performed under step-by-step realignment of the setup of the optical parametric amplification (OPA) source to establish the two above-mentioned border values: 110 and 150 fs. For our simulations, we used the input Gaussian pulse

$$\Psi(0, \tau) = a \exp(-\eta^2 \tau^2), \quad (11)$$

where  $a$  is the amplitude of the pulse envelope. From the FWHM definition,

$$\eta\tau = \eta \frac{t_{\text{FWHM}}}{2t_0} = \sqrt{\frac{\ln(2)}{2}} \approx 0.5887 \quad (12)$$

it follows that  $\eta = 1.1774t_0/t_{\text{FWHM}}$ , hence the respective values of the inverse-width parameter in Eq. (11) are  $\{\eta(150 \text{ fs}); \eta(110 \text{ fs})\} = \{(11.609/150); (11.609/110)\} =$

$\{0.0774; 0.1055\}$ . The energy of the pulse as a function of  $a$  and  $\eta$  can be expressed as

$$E = \int_{-\infty}^{+\infty} |A(z, t)|^2 dt = \frac{\kappa t_0}{\gamma} \sqrt{\frac{\pi}{2}} \frac{a^2}{\eta} = 14.739 \frac{a^2}{\eta} [\text{pJ}]. \quad (13)$$

The experimental work was carried out with the standard setup presented in detail in Refs. [12, 22]. Femtosecond pulses centered at 1700 nm were generated in an OPA pumped by the second harmonics of commercial Yb:KGW laser system (Pharos, Light Conversion) operating at 10 kHz repetition rate. The OPA allowed the tuning of the pulse wavelength in the range of 1500 – 1900 nm, which is an essential option for studying DCFs with different levels of the asymmetry. The propagation-constant mismatch decreases with the increase of the wavelength [11] therefore the DCF sample which featured poor switching performance at 1560 nm was studied in this work, using 1700 nm input pulses. The pulses were guided through a half-wave plate and polarizer representing a tunable attenuator and through a second half-wave plate to set the proper pulse polarization. The in-coupling and out-coupling of the beam were provided by two 40x microscope objectives mounted on 3D-positioners, securing submicron precision. The output of the fiber was monitored by an infrared camera imaging the output facet on its detector surface. Under the single-core excitation, series of camera images were registered by changing the energy of the excitation pulses in the range of 0.1 – 1.5 nJ separately for the fast and slow core excitation. Additionally, the recordings were repeated for different pulse widths achieved by tuning the OPA while simultaneously keeping the central wavelength at 1700 nm.

It is relevant to mention that the *linearized version* of the system of Eqs. (7) and (8) admits an exact solution for continuous-wave (CW) states, i.e., ones with constant amplitudes of the fields:

$$(\Psi_1)_{\text{CW}} = \Psi_0 \cos(K\zeta) e^{i(p\zeta - \Omega T)}, \quad (14)$$

$$(\Psi_2)_{\text{CW}} = \Psi_0 [A \cos(K\zeta) + iB \sin(K\zeta)] e^{i(p\zeta - \Omega T)}. \quad (15)$$

Here  $\Psi_0$  is an arbitrary constant amplitude and  $\Omega$  is an arbitrary frequency shift, which defines the family of the CW solutions. Further,  $p$  is the corresponding shift of the propagation constant,  $B$  is the relative amplitude of the waves in the two cores, and  $2\pi/K$  is the period of the power switching between the cores. The latter parameters are expressed in terms of  $\Omega$  as

follows:

$$A = - \left[ \sigma + \frac{\Omega}{2} (\alpha_1 - \alpha_2) \right] / (1 + \epsilon\Omega), \quad (16)$$

$$B = K / (1 + \epsilon\Omega), \quad (17)$$

$$p = -\frac{1}{2}\Omega^2 + \frac{\Omega}{2} (\alpha_1 - \alpha_2), \quad (18)$$

$$K^2 = (1 + \epsilon\Omega)^2 + \left[ \sigma + \frac{\Omega}{2} (\alpha_1 - \alpha_2) \right]^2. \quad (19)$$

In the absence of the group-velocity mismatch, i.e.,  $\alpha_1 - \alpha_2 = 0$ , this solution is tantamount to the previously known one [4]. The exact CW solution, given by Eqs. (14)-(19), is a novel finding. Actually, it can be obtained from the one known for  $\alpha_1 - \alpha_2 = 0$ , if the Doppler shift,  $(\alpha_1 - \alpha_2)\Omega$ , is added to the phase-velocity mismatch,  $2\sigma$ .

The asymmetry of the solution is characterized by the ratio of the amplitudes:

$$\frac{\max(|\Psi_2(\zeta)|)}{\max(|\Psi_1(\zeta)|)} = \sqrt{B^2 + K^2} \equiv \sqrt{1 + 2 \left[ \sigma + \frac{\Omega}{2} (\alpha_1 - \alpha_2) \right]^2}, \quad (20)$$

where index 2 represents the excited core. At  $\sigma = 0.3$  coupling efficiency is still high, as the ration of their amplitudes is equal to 1.086. Note that the asymmetry is cancelled at a specially chosen value of the frequency shift,

$$\Omega_0 = -2\sigma / (\alpha_1 - \alpha_2). \quad (21)$$

Lastly, in the absence of the group-velocity mismatch,  $\alpha_1 - \alpha_2 = 0$ , the simplified form of the exact solution admits a more sophisticated exact solution. It is a two-component chirped Gaussian pulse, localized (and, in the general case, moving) along the temporal coordinate, with two components periodically oscillating between the cores. These solutions also contain an arbitrary frequency shift  $\Omega$ , cf. Eqs. (14) and (15):



$$\begin{aligned}
(\Psi_1)_{\text{Gauss}} &= \Phi(\zeta) \cos\left(\sqrt{1+\sigma^2}\zeta\right) \\
&\times \exp\left(-\frac{1}{2}\varphi(z)(T+\Omega\zeta)^2 - i\Omega T - \frac{i}{2}\Omega^2\zeta\right), \tag{22}
\end{aligned}$$

$$\begin{aligned}
(\Psi_2)_{\text{Gauss}} &= \Phi(\zeta) \left[ -\sigma \cos\left(\sqrt{1+\sigma^2}\zeta\right) + i\sqrt{1+\sigma^2} \sin\left(\sqrt{1+\sigma^2}\zeta\right) \right] \\
&\times \exp\left(-\frac{1}{2}\varphi(z)(T+\Omega\zeta)^2 - i\Omega T - \frac{i}{2}\Omega^2\zeta\right), \tag{23}
\end{aligned}$$

where  $\varphi(z)$  and  $\Phi(z)$  are the following complex functions:

$$\varphi(z) = \frac{1}{W^2 + i\zeta}, \tag{24}$$

$$\Phi(z) = \frac{W\Psi_0}{\sqrt{W^2 + i\zeta}}, \tag{25}$$

with an arbitrary parameter  $W$  which determines the width of the Gaussian. The oscillation period between the cores is determined by the  $\zeta$ -dependence of the energies of components (22) and (23), cf. Fig. 7 below:

$$\left\{ \begin{array}{c} E_1(\zeta) \\ E_2(\zeta) \end{array} \right\} = \sqrt{\pi} |\Psi_0|^2 W \left\{ \begin{array}{c} \sin^2(\sqrt{1+\sigma^2}\zeta) \\ \sigma^2 + \cos^2(\sqrt{1+\sigma^2}\zeta) \end{array} \right\}. \tag{26}$$

Naturally, the total energy,  $E_1(\zeta) + E_2(\zeta)$ , stays constant in the course of the oscillations between the cores.

As concerns the frequency shift, it is related to the experimentally controllable shift  $\Delta\lambda$  of the carrier wavelength,  $\lambda_0$ . In physical units, the relation is

$$\Omega_{\text{phys-units}} \approx -\frac{2\pi c_0}{n\lambda_0^2} \Delta\lambda, \tag{27}$$

where  $c_0$  is the light speed in vacuum, and  $n$  is the refractive index. In the scaled form adopted above, the value is

$$\Omega = t_0 \Omega_{\text{phys-units}},$$

where  $t_0$  is the time unit defined in Eq. (10). Such simple analytical approach allows to evaluate the excitation wavelength effect on the coupling efficiency. In correspondence to our previous works [11] we observed reduced coupling

efficiency with decreasing excitation wavelength, therefore we performed the experimental study at 1700 nm instead of 1560 nm. Using equation (20) the same effect is predicted. Taking into consideration the positive value of  $\Delta\lambda$  tuning the wavelength from 1700 to 1560 nm and the negative value of group velocity mismatch  $\alpha_1 - \alpha_2$ , the shorter wavelength excitation causes reduced coupling efficiency.

#### 4. Numerical results for nonlinear propagation

In numerical simulations, we used pulses with two different widths at the FWHM level, 150 and 110 fs to match the experimental data. In the case of the Gaussian pulse, the corresponding values of the inverse pulse width, defined above, were  $\eta_1 = 0.077$  and  $\eta_2 = 0.11$ , respectively. Additionally, we investigated the effect of the mismatch in the effective refractive index to find optimal conditions for controllable switching performance. The propagation distance in the simulations was approximately 25 mm, and since the numerically calculated coupling length was 1.54 mm, it corresponds to about 8 periods of inter-core-coupling oscillations. It provides a possibility for analysis of the nonlinear dual-core propagation even beyond the experimentally studied 18 mm length, and puts the findings into a broader context. The simulation parameters (see Table 1) were selected from the mode solver analysis of the actual fiber structure. The use of these parameters allows direct comparison of the numerical results and experimental observations. In the nonlinear simulations, we considered both high-index- and low-index-core excitations, resulting in qualitative agreement with the experimental results in terms of the dependence of the propagation picture on the input energy. However, the considered simple model, which takes into account neither the linear dissipative effects (absorption, Rayleigh scattering), nor nonlinear ones (the stimulated Raman scattering and the generation of dispersive waves), cannot predict precise values of the switching energies. Therefore, presenting the numerical results, we refer to values of the pulse's amplitude, properly comparing the predictions with the experimental findings.

Preliminary experimental observations imply that introducing core asymmetry may lead to more stable and controllable switching performance (self-trapping of the pulse in the straight, initially populated or the opposite, initially empty channel, depending on the initial pulse amplitude) [22]. To put it in quantitative terms, in our simple model we varied the asymmetry parameter  $\sigma$  from 0.1 to 0.5 for the 150 fs pulse and classified outcomes

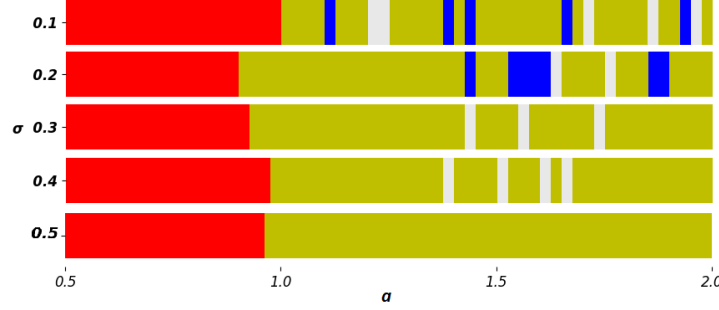


Figure 1: The pulse amplitude dependence of the dynamical propagation regime of the 150 fs Gaussian pulse in the case of the excitation of the low-index core, for different values of the propagation-constant mismatch,  $\sigma$ . The red color designates oscillatory behavior, when the final state depends on the actual length of the fiber. Blue means that, after a few initial oscillations, the pulse self-traps mostly in the excited (straight) channel; and yellow means the eventual self-trapping in the initially empty (cross) channel. White stripes were used to mark regions of low contrast, when signal in both channels is comparable, with small oscillations along propagation direction.

of the dynamics according to the dependence on the input pulse amplitude. Results are summarized in Figs. 1 and 2, which represent maps of the nonlinear dynamical scenarios in two cases, when the incident pulse excites either the low- or high-index core. The red color designates oscillatory behavior, when the final state depends on the actual length of the fiber. Blue means that, after a few initial oscillations, the pulse self-traps mostly in the excited (straight) channel; and yellow means the eventual self-trapping in the initially empty (cross) channel. We also marked (with white stripes) cases where we observed low contrast oscillatory behavior as a function of propagation distance. In the case of launching the pulse into the low-index core, at relatively low mismatch values ( $\sigma < 0.3$ ) we observe several alternations of the pulse trapping between both channels with increasing amplitude. At some amplitudes of input pulses, after a transient distance the signal becomes almost equally redistributed between two channels, performing low contrast oscillations (white regions). This outcome seems too fragile for the system to be used as an all-optical switch. However, at  $\sigma = 0.3$  they are not very frequent and the self-trapping takes place in the initially empty (cross) channel in a broad range of pulse amplitude. Such a behavior is quite natural, in view of the propensity of light to stay in a medium with higher refractive index. This outcome persists up to the highest analyzed amplitude of the input, i.e.

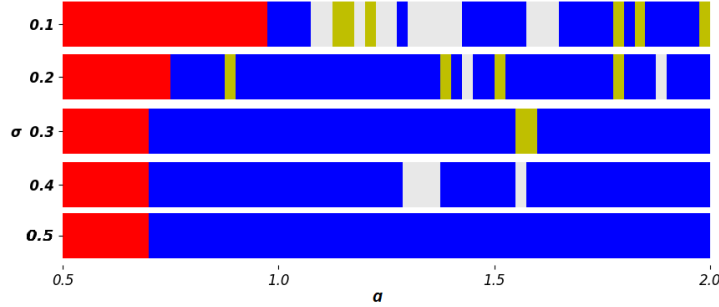


Figure 2: The pulse amplitude dependence of the dynamical propagation regime of the 150 fs Gaussian pulse in the case of the excitation of the high-index core, for different values of the propagation-constant mismatch,  $\sigma$ . The meaning of the color code is the same as in Fig. 1.

$a = 2.0$ , with some exceptions in narrow amplitude regions (white stripes), where equalized energies were predicted comparing the two channels.

In the case of higher mismatch, i.e.  $\sigma = 0.4$ , similar behavior is predicted, with some equalized dual-core energy distribution situations, but without retaining effect in the excited core. Thus, the low-index core excitation with 150 fs pulse width is not optimal for nonlinear switching performance. In the case of low asymmetry level ( $\sigma \leq 0.2$ ) the system is unstable: there are several transitions between the excited and cross core self-trapping state with increasing pulse amplitude. On the other hand, the higher asymmetry levels ( $\sigma > 0.2$ ) does not express self-trapping in the excited core; therefore, it does not support the effective nonlinear switching performance.

If the high-index core is initially excited, we again observe, at first, oscillations-straight (excited) channel trapping transition in the region of low energy. When the energy is higher, self-trapping occurs also in the empty (cross) channel. Such switching behavior to the cross-channel takes place in some narrow intervals of values of  $a$  (e.g., around 1.6 for the moderate asymmetry,  $\sigma = 0.3$ , which is shown in Fig. 2). Additionally, the trapping threshold decreases when the asymmetry increases. The reason for the latter effect is that the initial asymmetry of the fiber strengthened the trend to the self-trapping in the high-index core. The higher the initial asymmetry, the lower pulse energy is sufficient to induce additional asymmetry (discrete self focusing in terms of the channels) for establishing the self-trapping process. The yellow-colored areas disappear above  $\sigma = 0.3$ : only equalized dual-core energy effect is predicted (white stripes) in some narrow amplitude intervals.

The reason of this behavior in the case of highest asymmetry level is that the initial asymmetry already prevents the self-trapping in the cross-channel. Therefore, we conclude that 0.3 is the optimal mismatch value for switching in the case of 150 fs pulse width and high index core excitation, with clear self-trapping effect also in the non-excited channel. Thus we have a robust possibility to control the release of the pulse from a particular output port, regardless of whether the high or low index core is excited.

Analyzing the numerical results, we have concluded that the optimal value of the asymmetry parameter is 0.3 because for higher values of  $\sigma$  the self-trapping in the originally non-excited core is not more predicted. The switching dynamics is different when we excite the low- or high-index-core, with the cross or straight core self-trapping dominance occurring, respectively, in the former and latter cases. Furthermore, in the case when the fiber length in the experimental realization is equal to a multiple of the inter-core-oscillation period, a different peculiarity is observed in the transition between the inter-core oscillations and self trapping in the high-index core. As concerns the dominance of the output core, it is preserved in the case of the excitation of the high-index core, and, on the contrary, it is exchanged in the case of the low-index core excitation. In addition to that, the self-trapping may be switched between the two channels in narrow intervals of the initial amplitude, as may be concluded from Figs. 1 and 2 at low or moderate levels of the phase-velocity mismatch. The overall dynamics seems more stable in comparison to that observed in symmetric or weakly-asymmetric DCF studied before [13], where the diagram of dynamical regimes was more intricate, exhibiting stronger sensitivity to small variations both of the amplitude and pulse width.

## 5. Detailed comparison with experimental observations

Here, we aim to compare predictions of the above theoretical model with the experimental observations made in a nonlinear DCF, with the structure expressing optical parameters presented in Table 1, at wavelength 1700 nm. Numerical simulations were performed with parameters matched to the experimental setup, including the wavelength, shape and duration of the incident pulse.

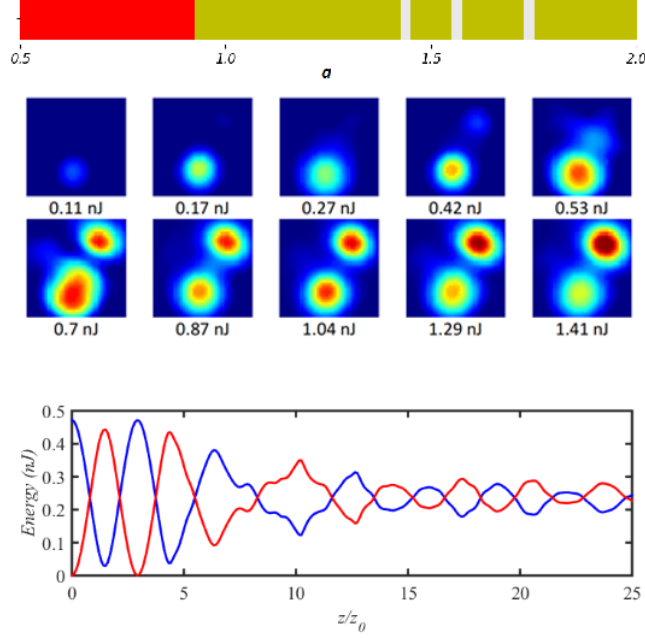


Figure 3: The comparison between the simulations diagram and experimental registration of the energy dependent output dual-core field distribution for the case of 150 fs Gaussian pulse launched into the low-index core. Bottom figure shows typical dynamics at the low contrast regions.

### 5.1. The core selection effect

In Fig. 3 we present the comparison between the theoretical model and experimental registration for the case of the low-index core excitation and the incident Gaussian pulse width  $t_{FWHM} = 150$  fs (the top panel of Fig. 3). Camera images demonstrate a single exchange of the dominant core around the critical value of the pulse energy of  $E = 0.87$  nJ. The simulation results predict the same one-step switching behavior from the inter-core oscillations to self-trapping in the cross core, which takes place at the amplitude  $a = 0.95$ . A narrow region of low contrast was predicted around  $a = 1.45, 1.55$  and  $1.75$ , and a similar effect is visible from the camera images. The bottom panel of Fig. 3 reports the distance-dependent dynamics of the energy distribution in both cores (blue - low-index/bottom core, red - high-index/top core) in the case of 150 fs pulse width and  $a = 1.65$ . It reveals that the propagation maintains an oscillatory character over the whole analyzed length, with an

exponential decrease of the peak power after each period  $z/z_0 = 1.65$ . It is an example of disturbing effect of the coupling on the soliton self-trapping mechanism. It takes place when the pulse cannot reach the self-trapping critical peak power, resulting in equalized field distribution between the two channels during the soliton self-compression process. As a consequence, the self-trapping process doesn't take place and the propagation maintains its harmonic features along the entire considered length. However, such effect require a certain ratio between the self-compression distance determined by the pulse amplitude and the coupling. Therefore, a slight tuning of the amplitude below or above the 1.65 level result in clear self-trapping effect. In the case of the high-index-core excitation, the images of the output fiber facet reveal a different result, viz., transient switching behavior at higher pulse energy, i.e. around 1.26 nJ (Fig. 4). Under further increasing of the pulse's energy, the same straight-core dominance was observed as in the linear propagation regime. The simulations predict similar outcome with the transient cross-core dominance effect around the amplitude level of 1.65.

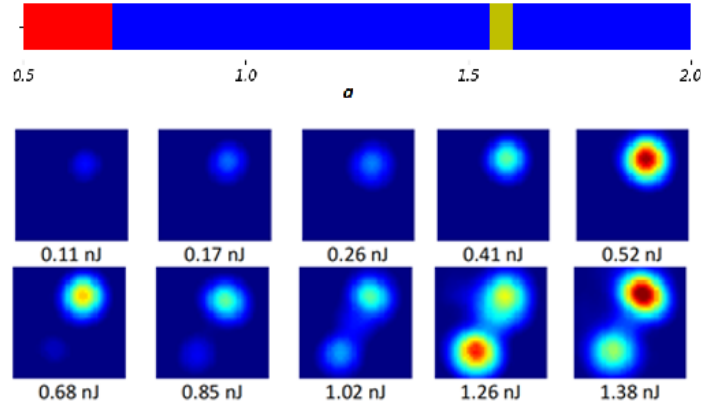


Figure 4: The comparison between the simulations diagram and experimental registration of the energy dependent output dual-core field distribution for the case of 150 fs Gaussian pulse launched into the high-index core.

The transition between the oscillatory and straight-core self-trapping, predicted by the simulations at the 0.72 level, is not observable experimentally because it does not change the core dominance in the output, due to choice of the fiber's length corresponding to an integer number of oscillation periods. Thus, the optimal level of the mismatch parameter identified in the

numerical study ( $\sigma = 0.3$ ) predicts similar switching performance as the experimental observation. It is a signature of the same optimal asymmetry level established in the experiment. It was ensured by tuning the wavelength of the excitation pulses to secure robust switching performance. Indeed, exciting the same DCF by C-band pulses resulted in poor switching performance [24]. However, the 1700 nm excitation improved it significantly; therefore, we set this wavelength also in our numerical analysis.

### 5.2. *The pulse-width effect*

Figure 5 presents the case of the low-index core excitation by pulses with 110 fs pulse width. It shows a more sophisticated dynamics than the one in case of 150 fs pulse width presented in Fig.2. It expresses three transitions between the output straight/cross core dominance at pulse energies 0.42 nJ, 0.69 nJ, and 1.03 nJ, considering both the simulation outcomes (top panel) and the experimental results (bottom panel). The numerical results predict transitions around amplitude levels 0.95, 1.8 and 1.95, which resembles the experimental observations with two dominance exchanges. The images in Figure 6 show the corresponding situation when the high-index core is excited with 110 fs pulse (bottom panel) and the predictions of the theoretical model for the same conditions at which the experiments were performed (top panel). The simulations exhibit three transitions: inter-core oscillations to self-trapping in the straight core at amplitude 0.75, then some low contrast lines transition to the straight core self-trapping state around level 1.85, followed by the inverse transition. The latter was not observed in the experiments due to limitations imposed on the pulse input energy, which should be kept below 1.5 nJ in order not to damage the input facet of the fiber. Furthermore, the oscillations to straight core self-trapping transition does not cause any exchange of the dominant core, as in the case of the results obtained for 150 fs pulse width (Fig.1). Therefore, from the camera images, one can see that only one straight/cross core transition is observed at 1.27 nJ, in correspondence to the numerical outcomes. between the inter-core oscillations and self-trapping in the cross core occurs, at the amplitude 0.95. In contrast, considering both the low and high-index core excitation cases, the 110 fs pulse width causes more complex changes in the pulse energy-dependent dual-core propagation dynamics. The reason of such character in the case of the shorter pulse is the linear decrease of the soliton order  $N$  with decreasing pulse width, according to equation



$$N^2 = \frac{\gamma P_0 T_0^2}{|\beta_2|}, \quad (28)$$

where  $P_0$  is the input pulse peak power and  $T_0$  the pulse width. The lower soliton order in the case of 110 fs pulse width reduces the disturbance of the pulse during the soliton fission process. Thus, the more preserved single pulse character supports more exchanges between the trapped channels with increasing pulse energy. The soliton self-compression effect, characterized by the factor  $F_c = 4.1N$  [23] is also more pronounced in the case of longer pulses. Consequently, the stronger selective self-focusing (which favors a particular channel) prohibits the transfer to the straight core at higher pulse amplitudes. Summarizing this sub-chapter, the 110 fs pulse width seems to be more advantageous because it enables high switching contrast between the channels based on self-trapping taking place in both of them. It is governed just by a slight change of the pulse amplitude and it is predicted in the case of both high- and low-index core excitation. The experimental observations confirmed these findings comparing 110 fs vs. 150 fs pulse excitation and considering both cores excitation.

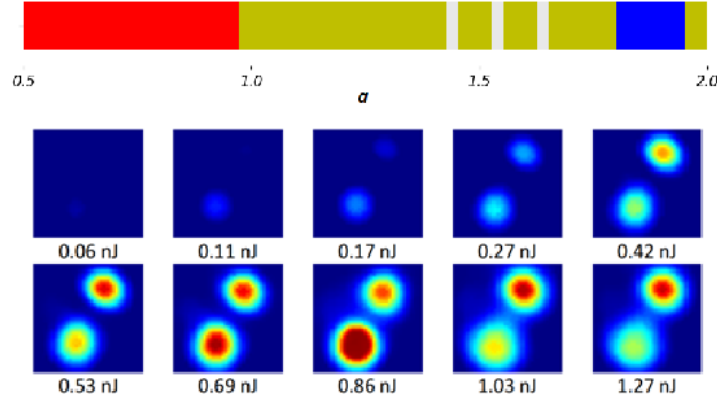


Figure 5: The comparison between the simulations diagram and experimental registration of the energy dependent output dual-core field distribution for the case of 110 fs Gaussian pulse launched into the low-index core.

Finally, in Figs.7-9 we illustrate the propagation-distance-dependent distribution in the both cores in the case of 110 fs pulse width, which signals the onset of the same sequence of three transitions as observed experimentally (bottom panel of Fig. 5). The top panel of Fig. 7 reveals that, at the low

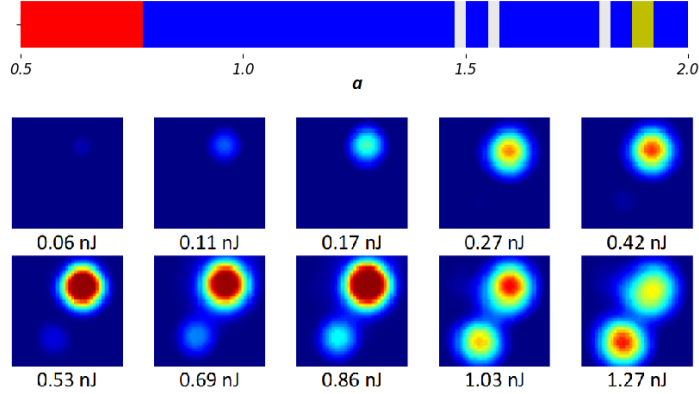


Figure 6: The comparison between the simulations diagram and experimental registration of the energy dependent output dual-core field distribution for the case of 110 fs Gaussian pulse launched into the high-index core.

amplitude level, when nonlinear effects are small, the propagation features oscillatory character in the whole studied propagation range [13]. In the propagation evolution graphs with higher pulse amplitudes, the harmonic behavior terminates after few initial oscillations due to the soliton self-compression and the subsequent self-trapping process [15]. According to our simulations, when the self-trapping commences, the core dominance is preserved in the whole subsequent range of the studied propagation lengths, including also the value which corresponds to the fiber length in the experiment. Another important aspect of the dual-core field-evolution plots is that they express nearly 100% transfer of the pulse's energy between the cores. It originates from the low level of the propagation constant mismatch parameter, 0.3, which, according to Eq. (20) describing various linear propagation approaches causes only a slight modification of the effective coupling constant, hence the coupling period remains similar to that for the zero mismatch. Black arrows indicate the observation point, which corresponds to the fiber length used in the experiment. All three transitions presented subsequently in Figs. 7-9 exhibit a clear exchange of the dominant cores following a slight increase of the pulse amplitude between the top and bottom panel. Accordingly, all of them have been identified experimentally by the camera monitoring the output fiber facet, and the corresponding pairs of camera images (0.27 - 0.42 nJ, 0.53 - 0.69 nJ, 0.86 - 1.03 nJ) exhibit convincing switching contrasts. Thus, the

experimental observations have confirmed the predictions of the numerical simulations, i.e. the three-transition character of the energy dependence for the 110 fs pulse width, in the case of low-index core excitation.

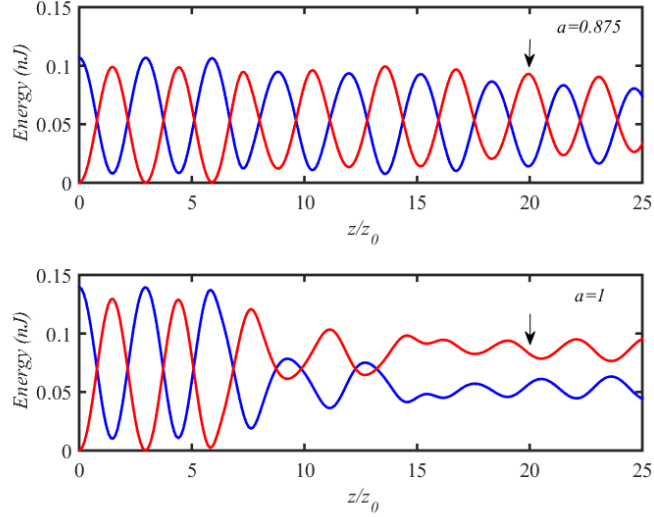


Figure 7: The dependence of the integral field energy on the propagation distance in both cores, as produced by the simulations. It shows the transition of oscillations to the cross core self-trapping for the input pulse amplitudes 0.875 (the upper panel) and 1.0 (the lower panel). Excitation pulses with width of 110 fs and Gaussian shape were launched into the low-index core of the fiber with asymmetry parameter  $\sigma = 0.3$ . The black arrow marks the length of the fiber in the experiment.

## 6. Conclusion

In conclusion, by means of systematic numerical simulations supported also by experimental findings, we have studied the switching dynamics in asymmetric nonlinear DCFs (dual-core fibers), with the propagation-constant mismatch between the guiding channels. We used a relatively simple numerical model taking into account all essential parameters of the fiber and input pulses, tailored to match the experimental conditions. An important control parameter is the inter-core difference of the effective refractive index determining the propagation-constant mismatch, which can be determined from the cross-section image of the DCF structure. However, such estimation bears high level of uncertainty, because it is defined by the overlap integrals

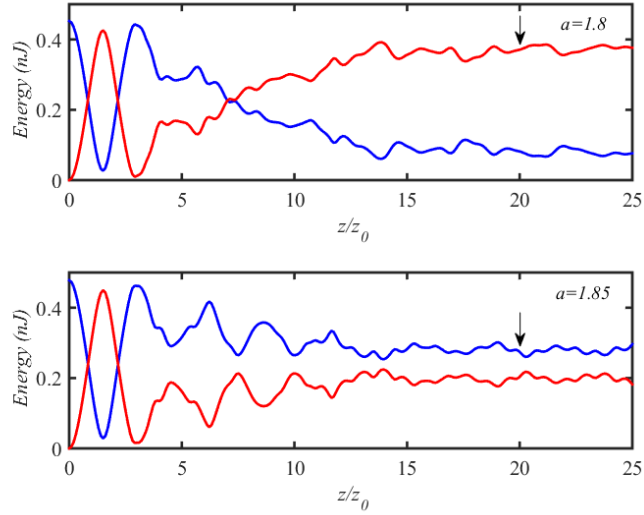


Figure 8: The dependence of the integral field energy on the propagation distance in both cores, as produced by the simulations. It shows the transition of the trapping from the cross core to the straight one for input pulse amplitudes 1.8 (the upper panel) and 1.85 (the lower panel). Excitation pulses with width of 110 fs and Gaussian shape were launched into the low-index core of the fiber with asymmetry parameter  $\sigma = 0.3$ .

of the field distribution in the two cores [4]. Therefore, its value is sensitive to fluctuations of the fiber microstructure along the propagation direction, even at the nanometer scale. On the other hand, in numerical simulations of the nonlinear propagation we introduce average mismatch parameter  $\sigma$  and determine its optimum value to be  $\sigma = 0.3$ . The simulations confirm experimental observations in terms of energy-dependent pulse dynamics when changing the excited core (low- or high-index), and tuning the inverse pulse width  $\eta$ . Note also that previously, good agreement was found in the study of the soliton propagation in the symmetric DCF [13]. Here the theoretical and experimental findings are summarized in back-to-back maps and camera images showing the optical field at the end of the fiber as functions of amplitude and energy of the excitation pulse, respectively. The comparison demonstrates only qualitative agreement between experimental findings and theoretical results, which were produced by the simplified model. As mentioned above, this study is similar to the case of the symmetrical coupler [13], where we could properly identify individual steps of the dominance exchange between the two guiding cores. However, in the recent work, we observe

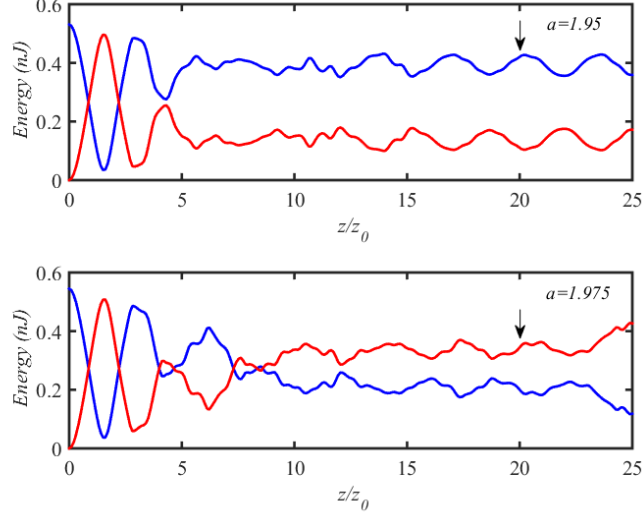


Figure 9: The dependence of the integral field energy on the propagation distance in both cores, as produced by the simulations. It shows the transition of the trapping from the straight core to the cross one for input pulse amplitudes 1.95 (the upper panel) and 1.975 (the lower panel). Excitation pulses with width of 110 fs and Gaussian shape were launched into the low-index core of the fiber with asymmetry parameter  $\sigma = 0.3$ .

much more robust and controllable switching dynamics, thanks to the effect of higher level of dual-core asymmetry. The outcomes as concerns the numerical and experimental approach alike, reveal a single transition between the inter-core oscillations and self-trapping in the cross core in the case of the low-index-core excitation and pulse width of 150 fs. In the case of the high-index-core excitation by pulses of the same width both simulations and experiments reveal two transitions (Fig.4), and the low-index-core excitation by 110 fs pulses reveal three transitions (Figs.5-6), following the increase of the pulse's amplitude and energy. The predictions of the numerical model are correct, with the fiber length of 18 mm, representing about 6 full dual-core oscillation periods.

These outcomes reveal an advantage of slight dual-core asymmetry, as compared to the totally symmetric DCF structures, in terms of more robust switching dynamics, which is resistant to small fluctuations of the input pulse's energy. It is a significant progress in the case of applications of all-optical binary operation, where the switching is controlled establishing two different input amplitude levels.

It is relevant to stress, that the identified optimal asymmetry level still represents just a slight perturbation on top of the propagation in the symmetric coupler, as observed in Figs. 7-9. Therefore, the experimental study required a low level of the dual-core asymmetry, which became available only recently, provided by new technology based on use of the high-index-contrast soft glass. Hence, the results offer an essential added value to the further designing of novel all-solid DCFs intended for all-optical switching purposes. We have also improved the numerical model: besides considering the propagation constant and group velocity mismatch between the guiding channels, the coupling coefficient dispersion was added as well. It turned out to be an efficient tool for analyzing the pulse-width effect on the switching in the femtosecond soliton-propagation regime. Further benefit of this work is the analytic solution of the mismatched coupler in the linear propagation regime. It confirms that: a) at  $\sigma = 0.3$  we observe only just a slight perturbation to the linear propagation in terms of coupling efficiency and period, b) with increasing wavelength the asymmetry is decreasing. In our numerical studies we went beyond the analytical approach, by adding the nonlinear and dispersion terms, however neglecting the higher-order nonlinear effects. Therefore the dynamics in our simulations, which is in agreement with the experimental observations at low energies, still preserve the features of the analytical solution and predicts the more robust nonlinear switching behavior at slight enhancement of the asymmetry.

Conditions concerning the pulse's energy and width, which are required of our approach, are in agreement with parameters of the commercial ultrafast oscillators. Thus, using our numerical tool, we can predict the proper level of the propagation-constant mismatch, taking into consideration the wavelength, pulse's width and top energy provided by such sources, in order to establish robust, high-contrast switching of the pulses. For example, it is possible to propose a mismatch parameter at 1560 nm, which will result in similar advantageous switching behavior as we obtained in this work performed at 1700 nm. Combining our novel specially designed dual-core fibers with such relatively cheap lasers opens the way for development of the synchronization of the ultrafast oscillators, sampling of data-carrying signals, or their redirection with the transfer rate exceeding 1 Tb/s. An additional asset of the model is its applicability to the design of fiber couplers with the appropriate mismatch, considering parameters of commercially available ultrafast laser sources.

## Acknowledgment

This work was supported by the Polish National Science Center under projects with No. 2020/02/Y/ST7/00136 (R.B.), 2016/22/M/ST2/00261 (M.T., R.B., M.L.) and 2019/33/N/ST7/03142 (M.L.), by the Vietnam Ministry of Education and Training (MOET) under Grant Number B2022-BKA-14 (N.V.H.), by the Austrian Science Fund (FWF) under Grant number I 5453-N (I.B., A.P., A.B.) and by Slovak Scientific Grant Agency through grant No. VEGA 2/0070/21 (I.B.) and, in part, by the Israel Science Foundation through grant No. 1695/22 (B.A.M). The authors declare no conflicts of interest.

## References

- [1] S. Jensen, *The nonlinear coherent coupler*, IEEE J. Quantum Electron. 18, 1580–1583, 1982.
- [2] A. A. Maier, *Optical transistors and bistable devices utilizing nonlinear transmission of light in systems with unidirectional coupled waves*, Sov. J. quantum Electron. 12, 1490–1494, 1982.
- [3] R. Hui, *Chapter 6 - passive optical components*, in *Introduction to Fiber-Optic Communications*, 1st ed, (Elsevier, 2020, pp. 209–297).
- [4] G. P. Agrawal, *Fiber couplers*, in *Applications of Nonlinear Fiber Optics*, (Academic Press, 2008, pp. 54–99).
- [5] S. Trillo, E. M. Wright, G. I. Stegeman, and S. Wabnitz, *Soliton switching in fiber nonlinear directional couplers*, Opt. Lett. 13, 672, 1988.
- [6] J. Herrmann, U. Griebner, N. Zhavoronkov, A. Husakou, D. Nickel, J. C. Knight, W. J. Wadsworth, P. S. Russell, and G. Korn, *Experimental evidence for supercontinuum generation by fission of higher-order solitons in photonic fibers*, Phys. Rev. Lett. 88, 1739011–1739014, 2002.
- [7] F. Luan, A. Yulin, J. C. Knight, and D. V. Skryabin, *Polarization instability of solitons in photonic crystal fibers*, Opt. Express 14, 6550, 2006.

- [8] X. He, K. Xie, and A. Xiang, *Optical solitons switching in asymmetric dual-core nonlinear fiber couplers*, Optoelectronics Adv. Mater. - Rapid Commun. 4, 3, March 2010 4,3, 284–286, 2010.
- [9] T. Uthayakumar, R. V. J. Raja, K. Nithyanandan, and K. Porsezian, *Designing a class of asymmetric twin core photonic crystal fibers for switching and multi-frequency generation*, Opt. Fiber Technol. 19, 556–564, 2013.
- [10] A. Govindarajan, B. Malomed, A. Mahalingam, and T. Uthayakumar, *Modulational instability in linearly coupled asymmetric dual-core fibers*, Appl. Sci. 7, 645, 2017.
- [11] L. Čurilla, I. Astrauskas, A. Pugžlys, P. Stajanca, D. Pysz, F. Uherek, A. Baltuska, and I. Bugar, *Nonlinear performance of asymmetric coupler based on dual-core photonic crystal fiber: Towards sub-nanojoule solitonic ultrafast all-optical switching*, Opt. Fiber Technol. 42, 39–49, 2018.
- [12] M. Longobucco, I. Astrauskas, A. Pugžlys, D. Pysz, F. Uherek, A. Baltuška, R. Buczynski, and I. Bugár, *Broadband self-switching of femtosecond pulses in highly nonlinear high index contrast dual-core fibre*, Opt. Commun. 472, 126043, 2020.
- [13] V. H. Nguyen, L. X. T. Tai, I. Bugar, M. Longobucco, R. Buczyński, B. A. Malomed, and M. Trippenbach, *Reversible ultrafast soliton switching in dual-core highly nonlinear optical fibers*, Opt. Lett. 45, 5221, 2020.
- [14] M. Longobucco, P. Stajanča, L. Čurilla, R. Buczynski, and I. Bugár, *Applicable ultrafast all-optical switching by soliton self-trapping in high index contrast dual-core fiber*, Laser Phys. Lett. 17, 025102, 2020.
- [15] M. Longobucco, J. Cimek, L. Čurilla, D. Pysz, R. Buczyński, and I. Bugár, *All-optical switching based on soliton self-trapping in dual-core high-contrast optical fibre*, Opt. Fiber Technol. 51, 48–58, 2019.
- [16] B. A. Malomed, *A variety of dynamical settings in dual-core nonlinear fibers*, in Handbook of Optical Fibers, (Springer, 2019, pp. 421–474).



- [17] W. Miao, F. Yan, and N. Calabretta, *Towards petabit/s all-optical flat data center networks based on wdm optical cross-connect switches with flow control*, J. Light. Technol. 34, 4066–4075, 2016.
- [18] M. Longobucco, I. Astrauskas, A. Pugžlys, D. Pysz, F. Uherek, A. Baltuška, R. Buczynski, and I. Bugár, *High contrast all-optical dual wavelength switching of femtosecond pulses in soft glass dual-core optical fiber*, J. Light. Technol. 39, 5111–5117, 2021.
- [19] M. Liu and K. S. Chiang, *Propagation of ultrashort pulses in a nonlinear two-core photonic crystal fiber*, Appl. Phys. B Lasers Opt. 98, 815–820, 2010.
- [20] J. Zhao, Z. Wang, Y. Liu, and B. Liu, *Switchable-multi-wavelength fiber laser based on dual-core all-solid photonic bandgap fiber*, Front. Optoelectron. China 3, 283–288, 2010.
- [21] J. H. Li, K. S. Chiang, and K. W. Chow, *Switching of ultrashort pulses in nonlinear high-birefringence two-core optical fibers*, Opt. Commun. 318, 11–16, 2014.
- [22] M. Longobucco, I. Astrauskas, A. Pugžlys, N. T. Dang, D. Pysz, F. Uherek, A. Baltuška, R. Buczyński, and I. Bugár, *Complex study of solitonic ultrafast self-switching in slightly asymmetric dual-core fibers*, Appl. Opt. 60, 10191, 2021.
- [23] G. P. Agrawal, *Pulse compression*, in *Applications of Nonlinear Fiber Optics*, (Academic Press, 2008, pp. 263–318).
- [24] M. Longobucco, J. Cimek, D. Pysz, R. Buczyński, and I. Bugár, *All-optical switching of ultrafast solitons at 1560 nm in dual-core fibers with high contrast of refractive index*, Opt. Fiber Technol. 63, 102154, 2021.